Contrasting different noise models for representing westerly wind bursts in a recharge oscillator model of ENSO

Georg A. Gottwald
School of Mathematics and Statistics, University of Sydney, Australia

Eli Tziperman
Department of Earth and Planetary Sciences and School of Engineering and Applied Sciences, Harvard University, Cambridge, MA, USA

Alexey Fedorov
Department of Earth and Planetary Sciences, Yale University, USA

Westerly wind bursts (WWBs) have long been known to have a major impact on the development of El Niño events. In particular, they amplify these events, with stronger events associated with a higher number of WWBs. We further find indications that WWBs lead to a more monotonically increasing evolution of warming events. We consider here a noise-driven recharge oscillator model of ENSO. Commonly, WWBs are represented by a state-dependent Gaussian noise which naturally reproduces the amplification of warm events. However, we show that many properties of WWBs and their effects on sea surface temperature (SST) are not well captured by such Gaussian noise. Instead, we show that conditional additive and multiplicative (CAM) noise presents a promising alternative. In addition to recovering the sporadic nature of WWBs, CAM noise leads to an asymmetry between El Niño and La Niña events without the need for deterministic nonlinearities. Furthermore, CAM noise generates a more monotonic increase of extreme warming events with a higher frequency of WWBs accompanying the largest events. This suggests that extreme warm events are better modelled by CAM noise. To cover the full spectrum of warm events we propose a conditional noise model in which the wind stress is modelled by additive Gaussian noise for sufficiently small SSTs and by additive CAM noise once the SST exceeds a certain threshold. We show that this conditional noise model captures the observed properties of WWBs reasonably well.

INTRODUCTION

Westerly wind bursts (WWBs) in the equatorial Pacific last a week or two, have a longitudinal scale of a thousand km, and have preceded and amplified every major El Niño event in the observed record [1]. WWBs trigger ocean Kelvin waves that accelerate the East Pacific warming [2]. While these are weather events, they are not completely random, and tend to occur when the equatorial SST begins to warm [3], therefore amplifying a developing El Niño [4]. Finally, WWBs occur more frequently during the active phase of the MJO [5, 6]. Because of this implied state-dependency, WWB events are commonly represented as a multiplicative Gaussian noise term in simplified ENSO models studying their role in El Niño events [e.g., 7, 8]. In this formulation, the red noise amplitude is multiplied by a Heaviside function of the temperature and by the East Pacific temperature itself, restricting the events to warmer than normal temperatures, and making sure the stochastic noise amplitude increases with the SST anomaly, as motivated by observational analysis [3]. This allows an excellent fit to the observed record [8, 9]. In this work, we provide an alternative to this stochastic forcing formulation, which provides an improved representation of the effects of WWBs on ENSO and which better resolves particular signatures of WWBs and their impact on major El Niño events.

To motivate our proposed formulation, consider Figure 1, which shows an inferred measure of the time-integrated wind stress associated with WWBs from a numerical simulation of a global configuration of the Community Atmospheric Model [10]. The measure attempts to represent the effect of these events on the ocean, including both their amplitude and their duration. The observed time series with its sporadic high-amplitude peaks resembles that of so called correlated additive and multiplicative (CAM) noise [11–14]. This suggests to replace the commonly employed Gaussian stochastic forcing by non-Gaussian CAM noise. As we will show, such CAM noise naturally reproduces the observed asymmetry between El Niño and La Niña events, without the inclusion of any deterministic nonlinearities designed to promote such asymmetry. Moreover, CAM noise will be shown to generate several of the signatures of major El Niño events. In particular, major El Niño events are the result of a sustained driving by several large amplitude WWBs [5, 6]. Furthermore, major El Niño events exhibit a more monotonic increase in their strength over the preceding year as we will show. Both of these features are well reproduced by an RO model driven by CAM noise, whereas the standard multiplicative Gaussian noise fails to capture them. This suggests that CAM noise

is a more appropriate noise model to model WWBs in a warm ocean environment, promoting large El Niño events, whereas colder oceanic environments are better captured by Gaussian noise. We therefore propose a conditional noise model in which the noise is Gaussian unless the SST exceeds a certain threshold when the noise switches to CAM noise. This conditional noise model will be shown to well reproduce the observed signatures of large El Niño events, while preserving the overall observed statistical properties of ENSO.

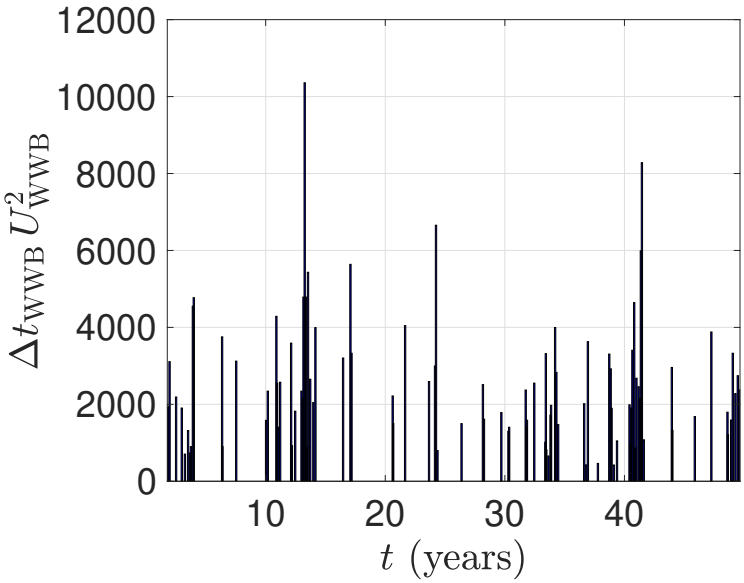

FIG. 1. An inferred measure of the time-integrated wind stress due to westerly wind bursts in a global climate model [CESM2, 15]. Shown is $\Delta t_{\mathrm{WWB}}\, U^2_{\mathrm{WWB}}$, where the WWB duration is given by Δt_{WWB} (in days) and the surface wind speed strength is U_{WWB} (in m/s).

The paper is organized as follows. In Section we introduce the recharge oscillator (RO) model [8, 16, 17], including a deterministic nonlinearity representing an asymmetric response of the SST to changes in the thermocline. Section introduces the stochastic forcing. We discuss additive and multiplicative noise and introduce a coloured Gaussian noise model as well as CAM noise. We show that the coloured Gaussian noise gives rise to Brownian motion when integrated whereas the CAM nosie gives rise to Lévy noise with abrupt jumps, which have the potential to trigger large El Niño events. Section numerically explores the effect of three noise (stochastic forcing) scenarios for representing WWBs in an RO model: (1) a standard Gaussian noise used as multiplicative noise based on the East Pacific SST, representing what is the emerging consensus in the ENSO literature; (2) a CAM noise, and finally, (3) a conditional noise that alternates between Gaussian noise for cold SST anomalies and CAM for positive anomalies. We argue that the conditional CAM noise may better capture the dynamics of large El Niño events. We conclude in Section with a discussion of our results.

METHODS

The recharge oscillator model

We consider the following recharge oscillator (RO) model [8, 16–18] for the Western Pacific thermocline depth anomaly h_w and the Eastern Pacific sea-surface temperature (SST) anomaly T_e,

$$\dot{T}_e = -r(T_e - \gamma h_e(t)) \tag{1}$$

$$\dot{h}_w = -\varepsilon(h_w + a\tau(t)), \tag{2}$$

where the Eastern Pacific thermocline depth is expressed as

$$h_e = h_w + d\,\tau, \tag{3}$$

with non-dimensional wind stress

$$\tau = bT_e + \nu\xi(t). \tag{4}$$

We set $d = 1\,m^3/N$ throughout. The parameters r and ε control the characteristic decay time scales for the SST and the thermocline depth, respectively, and a, b are positive constants. The noise $\xi(t)$ with amplitude $\nu > 0$ represents the effect of westerly wind bursts [8]. For westerly wind anomalies, $\xi > 0$, the noise acts to reduce the West Pacific thermocline depth h_w and amplifies the East Pacific SST T_e, and vice versa for $\xi < 0$. The RO model can be concisely written as [8],

$$\dot{T}_e = RT_e + F_1 h_w + \sigma_T\,\xi(t) \tag{5}$$

$$\dot{h}_w = -F_2 T_e - \varepsilon h_w - \sigma_h\,\xi(t), \tag{6}$$

where $R = r(\gamma b - 1)$ represents the Bjerknes feedback and $F_1 = r\gamma$ and $F_2 = ab\varepsilon$ are constants, and $\sigma_T = F_1\nu$ and $\sigma_h = F_1F_2/(R+r)\nu$ denote the amplitudes of the noise. Without stochastic driving (i.e., $\nu = 0$) the dynamics of (5)–(6) is that of a damped linear oscillator with frequency $\omega^2 = F_1F_2 - (\varepsilon + R)^2/$ and damping rate $\lambda = (\varepsilon - R)/2$.

We choose parameters such that one time unit in (5)–(6) corresponds to 1 month. We remark that tuning the parameters of the RO model to match observations of ENSO's variance, period, skewness, etc., introduces a biased set of parameters toward ENSO being too strongly damped [19], although that should not affect our focus here.

To account for the observed asymmetry that El Niño events are typically of a larger magnitude than La Niña events, the RO model can be extended to include a nonlinear term in the temperature equation [see 8, for a recent review]. Instead, we use in one of our three numerical experiments below a nonlinear response of the SST to the thermocline depth, motivated by the parameterization of subsurface temperature in the CZ model [20]. This involves employing a nonconstant response γ of the SST to changes in the thermocline,

$$\gamma = \begin{cases} \gamma_+ & \text{if } h_e \geq 0 \\ \gamma_- & \text{if } h_e < 0, \end{cases} \quad . \tag{7}$$

With $\gamma_+ > \gamma_-$, equation (1) implies a stronger effect of a positive thermocline depth anomaly on the SST than the effect of a negative thermocline depth anomaly. This enhances El Niño amplitudes relative to those of La Niña events, as observed. Alternatively, one could add quadratic nonlinearities (βT^2, with $\beta > 0$) in the temperature equation (1) to represent physical processes that favor the growth of El Niño relative to La Niña (e.g., [8, 21] for a systematic investigation of the impact of different nonlinear terms). Besides such deterministic nonlinearities, state-dependent stochastic drivers [18, 22, 23] and non-Gaussian noise [24, 25] were proposed as further dynamic ingredients to account for the observed asymmetry. In the following, we introduce several prototypical noise models. In Section we will discuss their effect on the dynamics of ENSO, including its asymmetry, within the RO model, and then combine them to generate a conditional noise that exhibits more realistic signatures consistent with observations.

Noise models

We consider both additive and multiplicative noise with

$$\nu = \nu_0 + \nu_1 \max(0, T_e). \tag{8}$$

Multiplicative noise with $\nu_2 \neq 0$ takes into account that atmospheric noise, such as westerly wind bursts (WWBs), occurs more frequently and with higher amplitude over a warmer equatorial ocean. Such multiplicative noise naturally introduces an asymmetry of larger El Niño events compared to La Niña events [9, 18, 22].

Additive noise with $\nu_1 = 0$ cannot generate the desired ENSO asymmetry for a Gaussian driving noise such as coloured Ornstein-Uhlenbeck (OU) processes [26]. However, as we will show, certain non-Gaussian noise models, such as CAM noise, can generate the asymmetry even when only applied additively. Correlated additive and multiplicative noise (CAM) is defined as the stochastic process governed by

$$d\xi = c_1\xi\,dt + (c_2\xi + c_3) \circ dW_1 + c_4\,dW_2. \tag{9}$$

Here, $W_{1,2}$ are independent Brownian motions (Wiener noise), with independent normally distributed random increments $W_i^{n+1} - W_i^n$, and $\circ$ denotes Stratonovich noise. This noise model naturally appears when modelling the effect of fast dynamic processes onto slower ones and has found numerous applications in atmospheric and climate dynamics [11–14, 27–29].

The noise model (9) contains both a purely Gaussian noise and a non-Gaussian noise as particular limits, depending on its parameters. For $c_2 = c_3 = 0$ and $c_1 < 0$, we have

$$d\xi = -|c_1|\xi\, dt + c_4\, dW_2, \tag{10}$$

and the CAM noise reduces to an Ornstein-Uhlenbeck noise with an asymptotic Gaussian distribution and zero mean.

However, for $c_1 < 0$ and $c_2 \neq 0$ CAM noise is non-Gaussian and lies in the domain of attraction of α-stable processes [30]. This means that if such a process is integrated in time, it generates random variables which are drawn from an α-stable distribution. Contrary, the central limit theorem ensures that if a Gaussian process is integrated in time, the resulting random variables are also distributed according to a Gaussian. Such α-stable processes or Lévy processes $L_{\alpha,\beta,\eta}$ are characterized by discrete jumps, and are parametrized by three parameters α, η and β. The stability parameter $\alpha \in (0, 2]$ determines the occurrence and size of the jumps. For $\alpha = 2$ we obtain a continuous Gaussian process without any discrete jumps. For $\alpha < 2$, however, the variance of such a process is not defined, as discrete jumps of arbitrary size have non-vanishing probability, and for $\alpha < 1$ even the mean ceases to exist. The skewness parameter $\beta \in [-1, 1]$ controls the direction of the jumps with $\beta = 1$ allowing for only positive jumps, $\beta = -1$ allowing for only negative jumps, $\beta = 0$ allowing for on average as many positive as negative jumps, and values of β in between quantifying the probability of having positive or negative jumps. The scale parameter η reduces to the variance for the Gaussian case with $\alpha = 2$. For more details on α-stable processes, we refer the reader to [31, 32].

For $c_4 \neq 0$ the mean of ξ is well-defined, and one has explicit expressions for the parameters of the resulting Lévy process α, β and η as functions of the parameters of the CAM process [30, 33]. For integrated CAM noise, the stability parameter α of the resulting α-stable process $L_{\alpha,\eta,\beta}$ is given by

$$\alpha = -2c_1/c_2^2, \tag{11}$$

the skewness parameter is given by,

$$\beta = \tanh\left(\frac{\pi c_3(\alpha - 1)}{2c_4}\right), \tag{12}$$

and the scale parameter η is given by

$$\eta = \left(\frac{2\cosh\left(\frac{\pi c_3(\alpha-1)}{2c_4}\right)}{c_2^{\alpha+1}\alpha N}\Gamma(1-\alpha)\cos\left(\frac{\pi}{2}\alpha\right)\right)^{\frac{1}{\alpha}},$$

with

$$N = 2\pi(2c_4)^{-\alpha}\,\frac{\Gamma(\alpha)}{c_2\Gamma(z)\Gamma(\bar{z})},$$
$$z = \frac{\alpha+1}{2} + i\frac{c_3(\alpha-1)}{c_4},$$

where the bar denotes the complex conjugate.

Figure 2 shows examples of CAM processes $\xi(t)$ and their integrals $\Xi = \int^t \xi(s)ds$. Panel (a) depicts a Gaussian Ornstein process with $c_1 = -2/3$, $c_4 = 0.7$, $c_2 = c_3 = 0$, which when integrated yields Brownian motion as shown in panel (c), in accordance with the central limit theorem. Panel (b) shows non-Gaussian CAM noise with intermittent unbounded peaks with $c_1 = 1.22$, $c_2 = 1.14$, $c_3 = 0.65$ and $c_4 = 0.8$, which, when integrated, lead to α-stable noise with jumps, as shown in panel (d). In the following, we will call noise obtained from (9) OU noise if $c_2 = c_3 = 0$ and $c_1 < 0$. We will use the term CAM noise only for those processes (9) that are not OU processes. For parameters of the CAM process that leads to α-stable noise with only positive jumps, i.e., $\beta = 1$, we see that jumps are caused by sporadic peaks of varying sizes of the CAM noise. These sporadic large-amplitude peaks will constitute our prototypical noise representation of WWBs. In our application, we need to limit the magnitude of the CAM noise for WWBs not to have an arbitrarily large amplitude. We will below replace the output of the CAM noise (9) by $\max(\xi, \theta)$, with $\theta = 3$ unless stated otherwise.

RESULTS

To examine the effect of the noise on ENSO as a representation of WWBs, we consider three noise models:

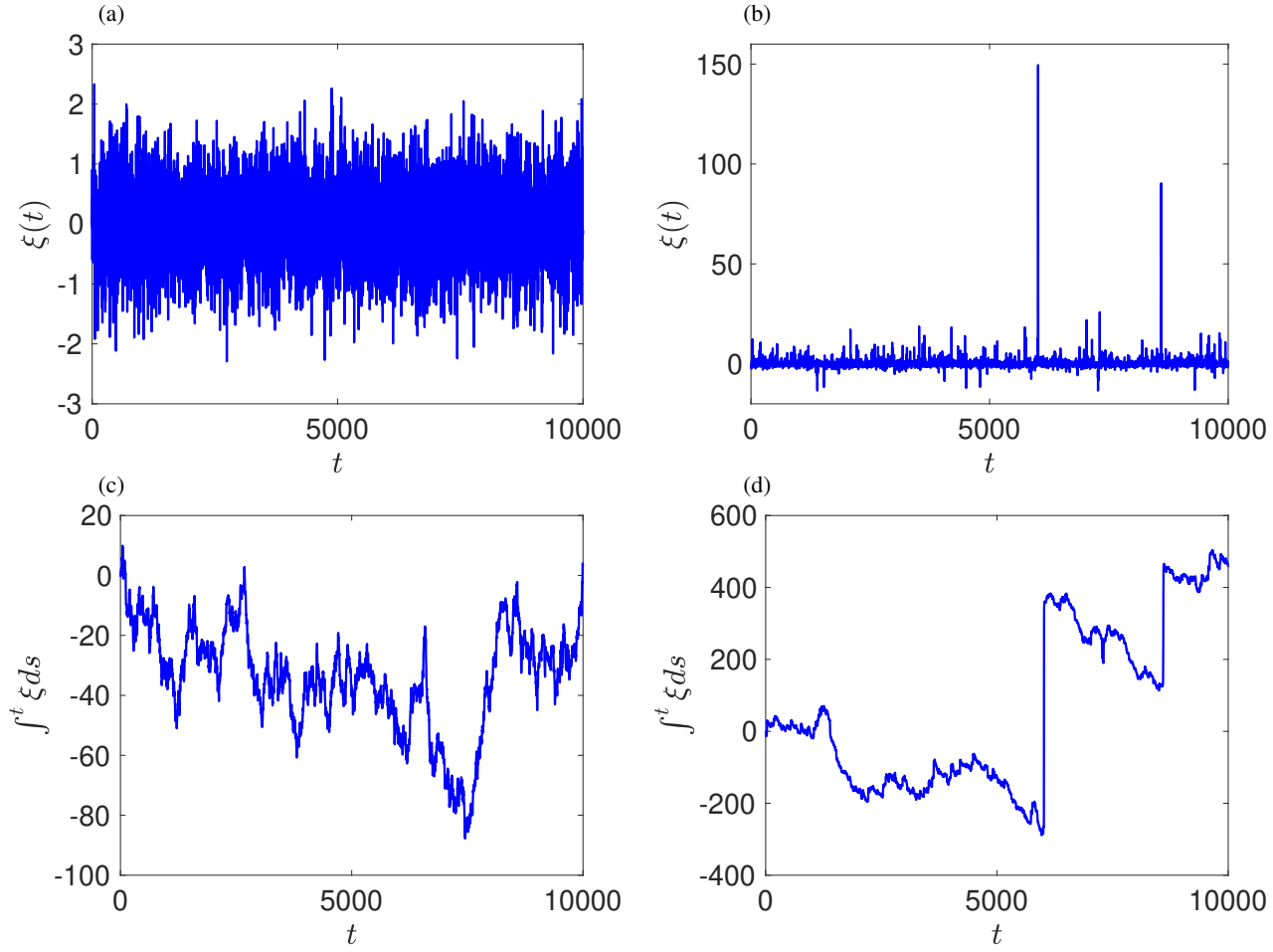

FIG. 2. (a) OU process with a characteristic decorrelation decay time of 4.9 days ($c_1 = -1.4$, $c_4 = 0.7$, $c_2 = c_3 = 0$). (b) CAM noise process with intermittent peaks ($c_1 = 1.22$, $c_2 = 1.14$, $c_3 = 0.65$ and $c_4 = 0.8$ with corresponding $\alpha = 1.88$ and $\beta = 0.81$). (c) and (d) show the integrals of (a) and (b), correspondingly.

(1) A multiplicative OU noise, a common representation of WWBs [8, 18, 22], denoted **OU**.

(2) An additive noise model with non-Gaussian CAM noise, denoted **CAM**.

(3) A conditional noise model, denoted **CON**, where we employ additive OU noise for negative SST anomaly, $T_e < 0$, and then allow for more intense WWBS modeled by adding CAM noise for $T_e > 0$.

Note that in **CON**, the noise is state-dependent, and can therefore be considered multiplicative noise, even if its amplitude is not proportional to the temperature as in **OU**.

Figure 3 shows the NINO3 index from 1871 until 2023 from the NOAA data set [34] where we subtracted the seasonal cycle and employed a moving average over a 4-month window. The focus of this work is large El Niño events, which we define to be those events with an NINO3 index larger than 1.5 °C. We expect such large events to be preceded by strong WWBs, consistent with the large El Niño events of 1997 and 2015 (marked by vertical gray lines in Figure 3), which were accompanied by particularly strong WWBs [35].

Our aim is to reproduce the statistical behaviour, as well as additional observed signatures associated with extreme El Niño events. Each of our three noise models is calibrated to reproduce the empirical histogram of the observed NINO3 time series, its power spectrum, and its variance and skewness, all based on the 153-year-long period from 1871 until 2023 (i.e., 1,836 months). We summarize the model parameters in Table I. For the conditional noise, we employ a window of three months to determine the persistence of an SST anomaly. For computational ease, in the RO model (1)–(2) the average over the past three months is calculated as the average over the last three monthly snapshots, rather than as an average over all time steps occurring

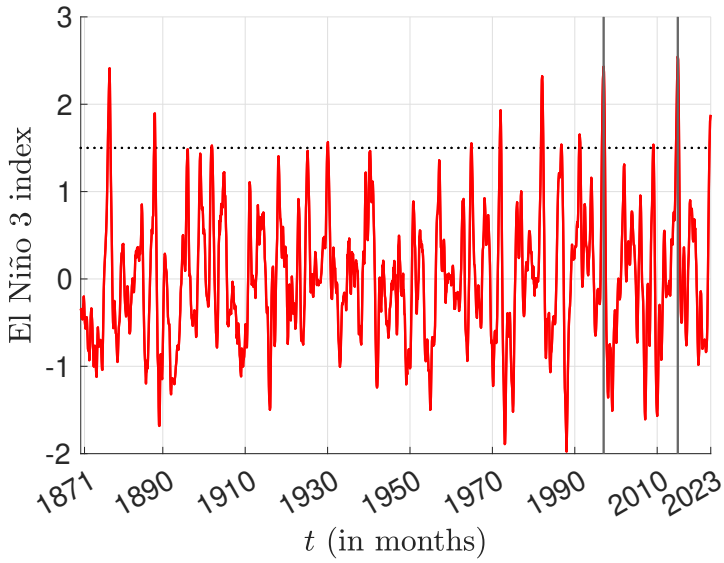

FIG. 3. Observed NINO3 index from 1871 until 2023. A moving average over 4 months was applied to observations from [34]. The horizontal line demarcates an index of 1.5, which we use to separate large El Niño events from normal ones. The vertical lines denote the years 1997 and 2015, for which the large El Niño events were accompanied by strong WWBs.

during the past three months. To match the empirical histogram for the conditional noise model (**CON**), we find we need to use the nonlinear SST response (7), which in effect shifts the histograms to higher values of the SST, enhancing its asymmetry.

Figure 4 shows a contour plot of the empirical 2D histogram of the variance and skewness for each 1,836-month-long segment of a 10^8 months-long simulation of the SST T_e for the RO model (1)–(2), together with the mean of the variance and skewness on the observed NINO3 index. Note that the nonzero skewness for the additive CAM noise is entirely generated by the symmetric CAM noise process, which favours positive amplitudes with $\beta = 0.8075$. Hence, CAM noise is capable of generating ENSO's asymmetry of having stronger El Niño events than La Niña events without any multiplicative noise or deterministic nonlinearities.

Figure 6 shows the corresponding histograms for the SST T_e and the power spectrum together with the corresponding curves for the observed NINO3 index. It is seen that all three noise models are capable of reproducing the global statistics reasonably well. Corresponding typical time series of the East Equatorial Pacific SST, T_e, are shown in Figure 5. The large sporadic peaks of the CAM noise as seen in Figure 2 give rise to large El Niño events and hence to a higher degree of asymmetry between El Niño and La Niña and a more skewed distribution compared to the OU process, even without any deterministic asymmetry promoting nonlinear SST response. We recall that we do not use the stochastic signal obtained from (9) directly but cap the signal to be bounded and not to exceed a threshold of $\theta = 3$. To better distinguish the capability of the respective noise models to reproduce the effect of large WWBs on the dynamics, we now seek more fine-grained signatures associated with large-amplitude El Niño events.

Observed strong El Niño events are accompanied by a sequence of WWBs. This is part of the positive feedback of warmer SSTs promoting the probability of the occurrence of WWBs, and WWBs intensifying the SST warming [e.g., 4]. Figure 7 shows the number of months that support a WWB during the 12-month period preceding an El Niño event. Strong WWBs are defined as large noise events with $\xi > 10/\nu_0$; for CON we choose the smaller of the two values for ν_0. We show results for the 20% largest and for the 20% smallest El Niño events (out of a long simulation of a total of 10^6 months). Consistent with the observation of strong El Niño events co-occurring with several WWBs, the temperature T_e of the strongest El Niño events is accompanied by a much larger number of WWBs for CAM and CON noise compared to small El Niño events (Figure 7b,c). This effect is still observable to some degree for the multiplicative OU process (Figure 7a), albeit to a much smaller degree.

We next present a further dynamical signature associated with large El Niño events. Figure 8 shows the evolution of the NINO3 index from the 12 months before the peak until the peak for the 22 largest El Niño events with NINO3 indices exceeding the threshold of 1.5. The four largest events, which include the two events from 1997 and 2015 that were preceded by unusually

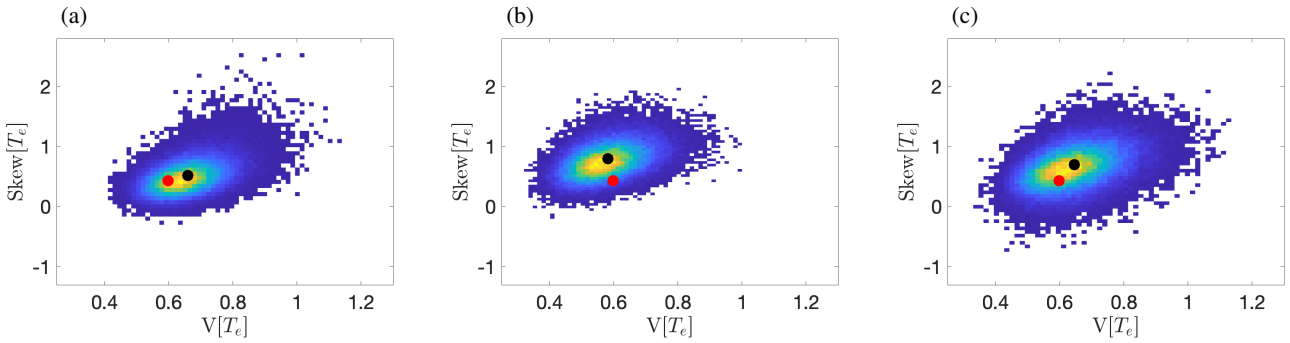

FIG. 4. Histograms of the variance and skewness of the SST for different driving noise models. The red dot demarcates the observed variance and skewness from the NINO3 index. The black dot is the average of a 10^8 month-long simulation of the recharge oscillator model (1)–(2). (a) OU, (b) CAM, (c) CON.

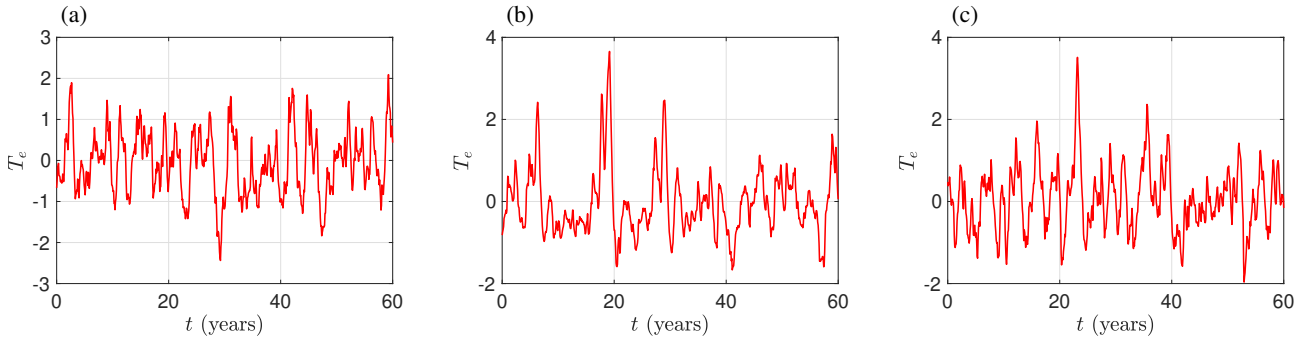

FIG. 5. Typical time series of the SST T_e obtained from the RO model (1)–(2), when driven by different noise models. (a) OU, (b) CAM, (c) CON.

strong WWBs, exhibit an increase in the year preceding the peak that is much less disrupted by downward NINO3 trends. In other words, the NINO3 time series leading to an El Niño event appears to be more monotonously increasing than for small events. To see if this feature of large WWB-dominated El Niños is reproduced by the three noise models, we rank all El Niño events in descending order and introduce a monotonicity measure μ_k for the kth largest El Niño event. The measure is zero if the NINO3 index monotonically increases in the last 12 months toward the peak, and it is positive for events where the increase toward the peak is not monotonous. We define,

$$\mu_k = \frac{1}{T_e^{(k)}(0) - T_e^{(k)}(-12)} \sum_{j=0}^{12} \left| \Delta_m T_e^{(k)}(j) \right| . \tag{13}$$

Here, $T_e^{(k)}(0)$ denotes the kth largest peak in T_e at peak time, and $T_e^{(k)}(-12)$ is the NINO3 index 12 months earlier for that peak. The operator Δ_m records negative increments in T_e, i.e., $\Delta_m T_e^{(k)}(j) = \min(T_e^{(k)}(j+1) - T_e^{(k)}(j), 0)$. We show in Figure 9 the monotonicity measure μ_k for the 100 largest El Niños recorded in a time series obtained by integrating the recharge oscillator model (1)–(2) for 1,000,000 months for the three noise models. For this purpose, El Niño events are defined as those peaks that are at least 12 months apart and have a duration of at least 4 months. It is seen that for the OU noise model, the 50 largest El Niño events have many more decreasing increments than for the CAM and CON models. We remark that the small sample size of the observations makes any statistical tests based on this measure hard, but the qualitative picture emerging from Figure 8 is compelling.

Recall that, contrary to the OU and the CAM noise model, the CON noise model involves an asymmetric response of the SST with $\gamma_1 \neq \gamma_2$. An obvious question is, if the observed behaviour depicted in Figures 7(c) and 9(c) is due to this asymmetric response rather than to the proposed conditional CAM noise model. To clarify this, we show in Figure 10 the monotonicity measure and the empirical histogram of the number of large noise amplitude events occurring during warm events for a conditional noise with a symmetric response (and adjusted noise amplitudes ν_0 to match the observed power spectrum as well as the implied variance and skewness of T_e). It is clearly seen that the conditional noise model with a symmetric response also exhibits the characteristic behaviour observed for real WWBs. The asymmetric response is required, however, to allow for a better approximation of the empirical histogram of the temperature (cf. Figure 6 (c)); a symmetric response leads to a histogram

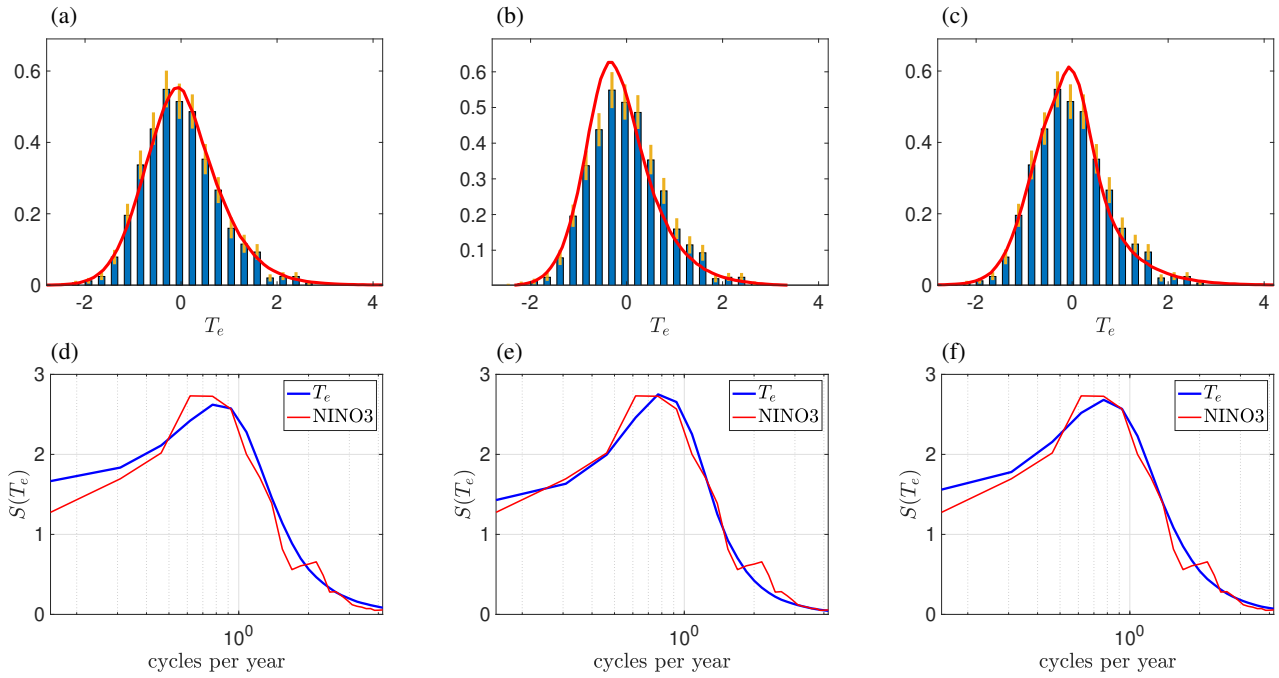

FIG. 6. (Top panels) Histograms of the observed NINO3 index from 1871 until 2023 with a monthly resolution and with the seasonal cycle removed (blue bars) and of the solution of the RO model (1)–(2) shown by continuous curves, for the three noise models, (a) OU, (b) CAM, (c) CON. We show the 5th and 95th percentile confidence levels for the NINO3 index data as bars (beige) estimated from 10,000 bootstrapped samples. (Bottom panels) Power spectra $S(T_e)$ of the observed NINO3 index from 1871 until 2023 with a monthly resolution and with the seasonal cycle removed (green) and of the solution of the RO model (1)–(2) for the three noise models (d) OU, (e) CAM, (f) CON. A Welch window of 16 years was employed.

shifted to smaller temperatures (not shown).

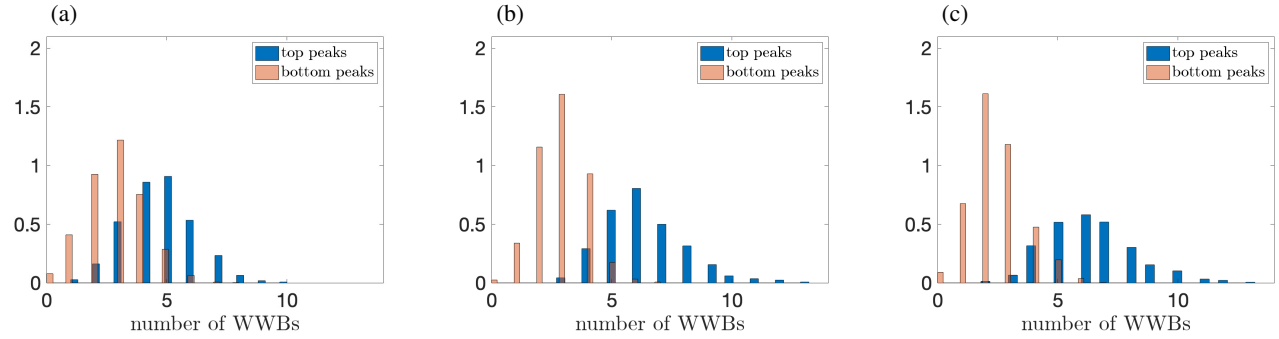

FIG. 7. Empirical histogram of the number of large noise amplitude events with $\xi > 10/\nu_0$ occurring in the 12 months preceding a warm event in the RO model (1)–(2). Shown are the empirical histograms for the largest and smallest fifth of El Niño events (with a duration of at least 4 months). Parameters as in Figure 4. (a) OU, (b) CAM, (c) CON.

CONCLUSIONS

We explored three noise models for representing the effects of WWBs on ENSO in an RO model. One is multiplicative **OU** noise, a choice often used in the literature for this purpose. Another is based on **CAM** noise, characterized by the occurrence of sporadic large peaks, motivated by the appearance of WWB amplitudes (Figure 1). And a final one that conditionally switches from OU for negative NINO3 to CAM for positive NINO3 (**CON**). All three models were able to explain the spectrum, the empirical histogram, the variance and the skewness of the observed NINO3 time series. We introduced two additional measures based on observed qualitative behavior of large El Niño events that are typically preceded by multiple WWBs. In particular, we

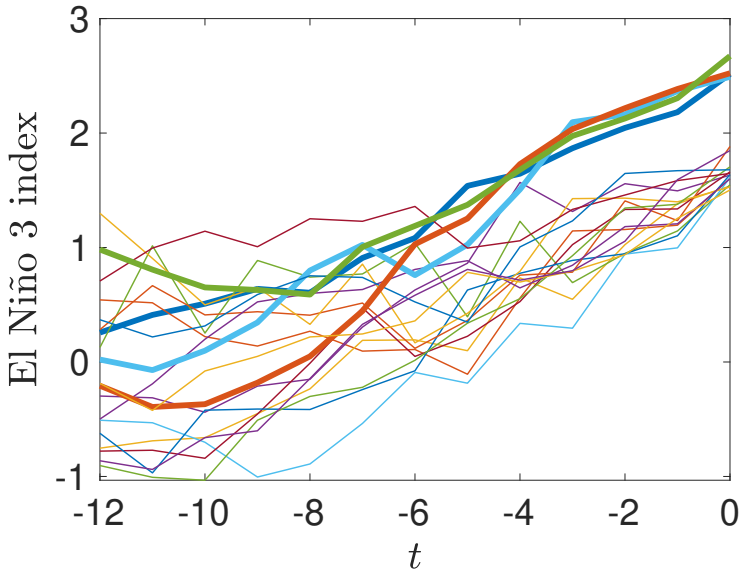

FIG. 8. Timeseries segments of NINO3 index of El Niño peaks, with the NINO3 index larger than 1.5. These are segments of the full timeseries seen in Figure 3, that are plotted from 12 months before the peak until the peak. The thick lines depict the four largest El Niño events in the observed record. This figure demonstrates that the NINO3 tends to increase monotonously for the largest events, motivating the monotonicity measure introduced in (13).

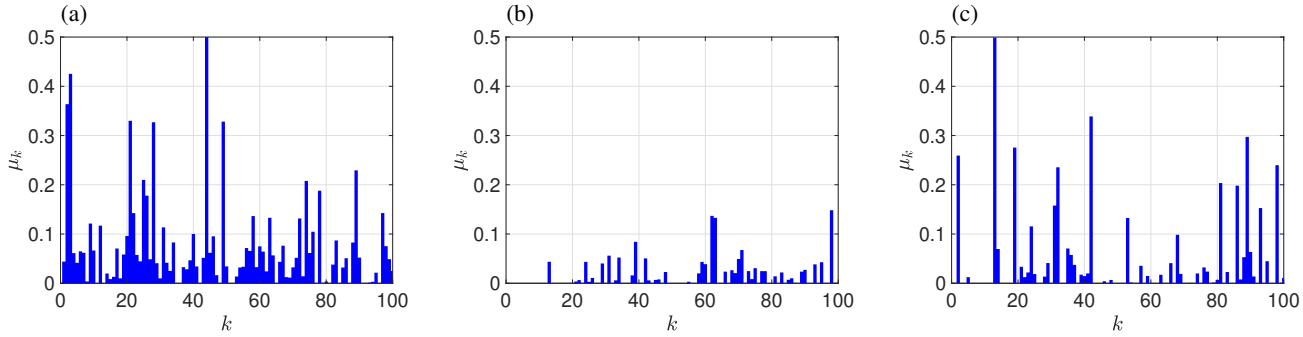

FIG. 9. Monotonicity measure μ for the 100 largest peaks in T_e for the RO model (1)–(2) with different driving noise models. (a) OU, (b) CAM, (c) CON.

considered the number of WWBs that precede large peaks and the monotonicity of the NINO3 increase toward the peak of El Niños.

Our numerical results suggest OU noise may be an appropriate forcing leading to normal El Niño events of small and moderate amplitude. Whereas we find that CAM noise is better suited to generate high-amplitude events, accounting for their monotonicity and larger number of WWBs preceding them. Our proposed conditional noise combines these two noise models to construct a noise model that accounts for both, small and large amplitude El Niño events, allowing for a better representation of WWBs, better reproducing the overall statistical features of ENSO as well as the observed qualitative behaviour of large amplitude El Niño events.

Further exploration of this idea using more realistic climate models seems an appropriate future direction.

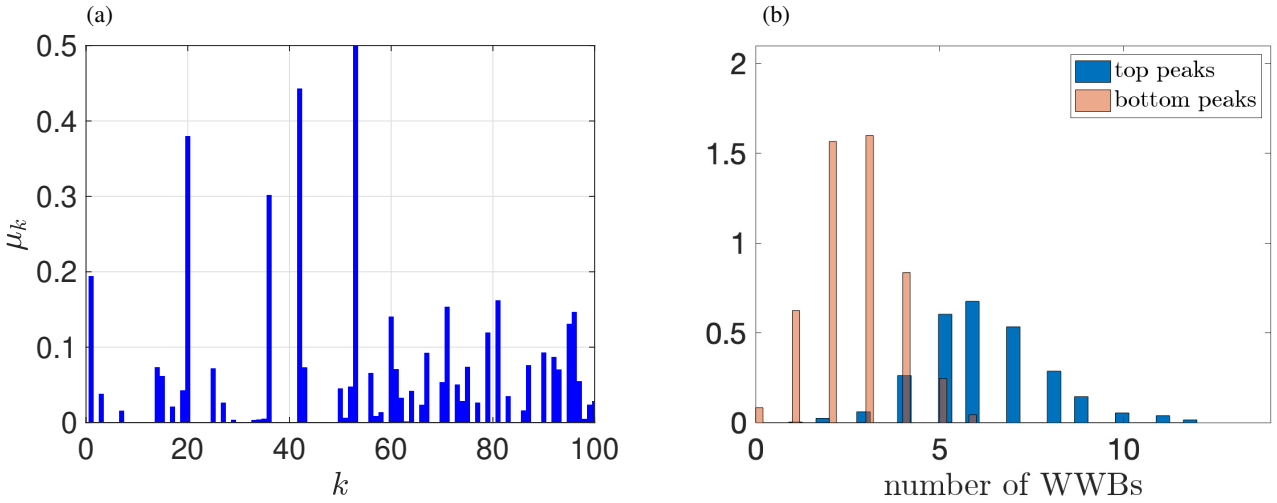

FIG. 10. (a) Monotonicity measure μ for the 100 largest peaks in T_e and (b) empirical histogram of the number of large noise amplitude events with $\xi > 10/\nu_0$ occurring in the 12 months preceding a warm event for the RO model (1)–(2) driven by a conditional noise model with all parameters as for CON but with a symmetric response $\gamma_1 = \gamma_2 = 0.08$ and adjusted noise amplitudes $\nu_0 = 17.5$ for the OU noise component and $\nu_0 = 5.4$ for the CAM component.

	multiplicative OU	**additive CAM**	**conditional OU/CAM**
r	0.28	0.25	0.17
ε	$1/2.7$	$1/2.7$	$1/2.7$
a	0.41	0.41	0.33
b	14	14	14
γ_+	0.088	0.09	0.08
γ_-	0.088	0.09	0.0728
ν_0	20	6	21/6.5
ν_1	0.2791	0	0
c_1	-1.4	-1.22	$-1.4/-1.19$
c_2	0	1.14	0/1.12
c_3	0	0.65	0/1.2
c_4	0.7	0.8	0.7/1.1

TABLE I. Parameters for the RO model (1)–(2) and the noise models (9). Here the units are as follows: $[r] = 1/\text{month}$, $[\varepsilon] = 1/\text{month}$, $[a] = m^3/N$, $[b] = 1/K$, $[\gamma_\pm] = K/m$, $[\nu_0] = 1$, $[\nu_1] = 1/K$.

APPENDIX: MODEL PARAMETERS

ACKNOWLEDGMENTS

AF and ET were funded by the Department of Energy (DOE) Office of Science Biological and Environmental Research grant DE-SC0023134. ET is also funded by the Harvard Dean's Competitive Fund for Promising Scholarship, and thanks the Weizmann Institute of Science for its hospitality during parts of this work.

[1] G. A. Vecchi and D. E. Harrison. Westerly wind events in the tropical pacific, 1986 1995: A atlas from the ECMWF operational surface wind fields. Technical report, NOAA/Pacific Marine Environmental Laboratory, 1997.

[2] William S. Kessler, Michael J. McPhaden, and Klaus M. Weickmann. Forcing of intraseasonal Kelvin waves in the equatorial Pacific. *Journal of Geophysical Research: Oceans*, 100(C6):10613–10631, 1995.

[3] Eli Tziperman and Lisan Yu. Quantifying the dependence of westerly wind bursts on the large-scale tropical Pacific SST. *Journal of Climate*, 20(12):2760 – 2768, 2007.

[4] Ian Eisenman, Lisan Yu, and Eli Tziperman. Westerly wind bursts: ENSO's tail rather than the dog? *Journal of Climate*, 18(24):5224 – 5238, 2005.

[5] Andrew M. Chiodi, D. E. Harrison, and Gabriel A. Vecchi. Subseasonal atmospheric variability and El Niño waveguide warming: Observed effects of the madden–julian oscillation and westerly wind events. *Journal of Climate*, 27(10):3619 – 3642, 2014.

[6] Yu Liang and Alexey V. Fedorov. Linking the Madden–Julian oscillation, tropical cyclones and westerly wind bursts as part of El Niño development. *Climate Dynamics*, 57(3):1039–1060, 2021.

[7] Cristina L. Perez, Andrew M. Moore, Javier Zavala-Garay, and Richard Kleeman. A comparison of the influence of additive and multiplicative stochastic forcing on a coupled model of ENSO. *Journal of Climate*, 18(23):5066 – 5085, 2005.

[8] J. Vialard, F.-F. Jin, M. J. McPhaden, A. Fedorov, W. Cai, S.-I. An, D. Dommenget, X. Fang, M. F. Stuecker, C. Wang, A. Wittenberg, S. Zhao, F. Liu, S.-K. Kim, Y. Planton, T. Geng, M. Lengaigne, A. Capotondi, N. Chen, L. Geng, S. Hu, T. Izumo, J.-S. Kug, J.-J. Luo, S. McGregor, B. Pagli, P. Priya, S. Stevenson, and S. Thual. The El Niño Southern Oscillation (ENSO) recharge oscillator conceptual model: Achievements and future prospects. *Reviews of Geophysics*, 63(1):e2024RG000843, 2025.

[9] Sooman Han, Alexey V. Fedorov, and JÃ©rÃ´me Vialard. Realistic ENSO dynamics requires a damped nonlinear recharge oscillator. *Journal of Climate*, 39(1):77 – 101, 2026.

[10] Andrew J Conley, Rolando Garcia, Doug Kinnison, Jean-Francois Lamarque, Dan Marsh, Mike Mills, Anne K Smith, Simone Tilmes, Francis Vitt, Hugh Morrison, et al. Description of the NCAR community atmosphere model (CAM 5.0). *NCAR technical note*, 3, 2012.

[11] Philip Sura and Prashant D. Sardeshmukh. A global view of non-Gaussian SST variability. *Journal of Physical Oceanography*, 38(3):639–647, 2008.

[12] Prashant D. Sardeshmukh and Philip Sura. Reconciling non-Gaussian climate statistics with linear dynamics. *Journal of Climate*, 22(5):1193–1207, 2009.

[13] Cécile Penland and Prashant D. Sardeshmukh. Alternative interpretations of power-law distributions found in nature. *Chaos: An Interdisciplinary Journal of Nonlinear Science*, 22(2):023119, 2012.

[14] Prashant D. Sardeshmukh and Cécile Penland. Understanding the distinctively skewed and heavy tailed character of atmospheric and oceanic probability distributions. *Chaos: An Interdisciplinary Journal of Nonlinear Science*, 25(3):036410, 2015.

[15] G. Danabasoglu, J.-F. Lamarque, J. Bacmeister, D. A. Bailey, A. K. DuVivier, J. Edwards, L. K. Emmons, J. Fasullo, R. Garcia, A. Gettelman, C. Hannay, M. M. Holland, W. G. Large, P. H. Lauritzen, D. M. Lawrence, J. T. M. Lenaerts, K. Lindsay, W. H. Lipscomb, M. J. Mills, R. Neale, K. W. Oleson, B. Otto-Bliesner, A. S. Phillips, W. Sacks, S. Tilmes, L. van Kampenhout, M. Vertenstein, A. Bertini, J. Dennis, C. Deser, C. Fischer, B. Fox-Kemper, J. E. Kay, D. Kinnison, P. J. Kushner, V. E. Larson, M. C. Long, S. Mickelson, J. K. Moore, E. Nienhouse, L. Polvani, P. J. Rasch, and W. G. Strand. The Community Earth System Model Version 2 (CESM2). *Journal of Advances in Modeling Earth Systems*, 12(2):e2019MS001916, 2020.

[16] Fei-Fei Jin. An equatorial ocean recharge paradigm for ENSO. Part I: Conceptual model. *Journal of the Atmospheric Sciences*, 54(7):811–829, April 1997.

[17] Gerrit Burgers, Fei-Fei Jin, and Geert Jan van Oldenborgh. The simplest ENSO recharge oscillator. *Geophysical Research Letters*, 32(13), 2005.

[18] Fei-Fei Jin, L. Lin, A. Timmermann, and J. Zhao. Ensemble-mean dynamics of the ENSO recharge oscillator under state-dependent stochastic forcing. *Geophysical Research Letters*, 34(3), 2007.

[19] Elle Weeks and Eli Tziperman. Is ENSO a damped or a self-sustained oscillation?, 2025.

[20] Stephen E. Zebiak and Mark A. Cane. A model El Niño Southern Oscillation. *Monthly Weather Review*, 115(10):2262 – 2278, 1987.

[21] Fangyu Liu, Jérôme Vialard, Alexey V. Fedorov, Christian Éthé, Renaud Person, Wenjun Zhang, and Matthieu Lengaigne. Why do oceanic nonlinearities contribute only weakly to extreme El Niño events? *Geophysical Research Letters*, 51(11):e2024GL108813, 2024.

[22] Aaron Levine, Fei Fei Jin, and Michael J. McPhaden. Extreme noise–extreme El Niño: How state-dependent noise forcing creates El Niño–La Niña asymmetry. *Journal of Climate*, 29(15):5483 – 5499, 2016.

[23] Aaron F. Z. Levine and Fei Fei Jin. A simple approach to quantifying the noise–ENSO interaction. Part I: deducing the state-dependency of the windstress forcing using monthly mean data. *Climate Dynamics*, 48(1):1–18, 2017.

[24] M. Bianucci. Analytical probability density function for the statistics of the ENSO phenomenon: Asymmetry and power law tail. *Geophysical Research Letters*, 43(1):386–394, 2016.

[25] Marco Bianucci, Antonietta Capotondi, Silvia Merlino, and Riccardo Mannella. Estimate of the average timing for strong El Niño events using the recharge oscillator model with a multiplicative perturbation. *Chaos: An Interdisciplinary Journal of Nonlinear Science*, 28(10):103118, 10 2018.

[26] Grigorios A Pavliotis. *Stochastic Processes and Applications*. Springer, 2016.

[27] Andrew J. Majda, Christian Franzke, and Daan Crommelin. Normal forms for reduced stochastic climate models. *Proceedings of the National Academy of Sciences*, 106(10):3649–3653, 2009.

[28] G.A. Gottwald, Daan Crommelin, and Christian Franzke. Stochastic climate theory. In Christian L. E. Franzke and Terence J. O'Kane, editors, *Nonlinear and Stochastic Climate Dynamics*, pages 209–240. Cambridge University Press, Cambridge, 2017.

[29] Georg A. Gottwald. A model for Dansgaard-Oeschger events and millennial-scale abrupt climate change without external forcing. *Climate Dynamics*, 56(1-2):227–243, 2021.

[30] Rachel Kuske and Joseph B. Keller. Rate of convergence to a stable law. *SIAM Journal on Applied Mathematics*, 61(4):1308–1323, 2001.

[31] David Applebaum. *Lévy processes and stochastic calculus*, volume 116 of *Cambridge Studies in Advanced Mathematics*. Cambridge University Press, Cambridge, second edition, 2009.

[32] Alexei V. Chechkin, Ralf Metzler, Joseph Klafter, and Vsevolod Yu. Gonchar. Introduction to the theory of Lévy flights. In Reiner Klages, Guenter Radons, and Igor M. Sokolov, editors, *Anomalous Transport*, pages 129–162. Wiley-VCH Verlag GmbH & Co. KGaA, 2008.

[33] William F. Thompson, Rachel A. Kuske, and Adam H. Monahan. Reduced α-stable dynamics for multiple time scale systems forced with correlated additive and multiplicative Gaussian white noise. *Chaos: An Interdisciplinary Journal of Nonlinear Science*, 27(11):113105, 2017.

[34] N. A. Rayner, D. E. Parker, E. B. Horton, C. K. Follandamd L. V. Alexander, D. P. Rowelland E. C. Kent, and A. Kaplan. Global analyses of sea surface temperature, sea ice, and night marine air temperature since the late nineteenth century. *J. Geophys. Res.*, 108 (D14), 2003.

[35] Martin Puy, Jérôme Vialard, Matthieu Lengaigne, Eric Guilyardi, Pedro N. DiNezio, Aurore Voldoire, Magdalena Balmaseda, Gurvan Madec, Christophe Menkes, and Michael J. Mcphaden. Influence of westerly wind events stochasticity on El Niño amplitude: the case of 2014 vs. 2015. *Climate Dynamics*, 52(12):7435–7454, 2019.